The Effect of UV Irradiation on Antimony-Doped Tin Dioxide Thin Films Derived from Methacrylic Acid Modified Precursors

T. Kololuoma,*,† L.-S. Johansson,‡ J. M. Campbell,‡ A. Tolonen,§ M. Halttunen,† T. Haatainen,|| and J. T. Rantala⊥

VTT Electronics, Kaitoväylä 1, FIN-90570 Oulu, Finland, Helsinki University of Technology, Centre for Chemical Analysis, P.O. Box 6100, FIN-02015 TKK, Finland, University of Oulu, Department of Chemistry, P.O. Box 3000, FIN-90014 Oulun Yliopisto, Finland, VTT Information Technology, P.O. Box 1101, FIN-02044 VTT, Finland, and GuideOptics Oy, P.O. Box 114, FIN-90571 Oulu, Finland

Received June 11, 2002

In this paper, we report the effect of direct UV photopatterning on the compositional and morphological characteristics, and hence the conductivity, of antimony-doped tin dioxide thin films (55−70 nm) prepared using wet-deposition techniques. Direct UV photopatternability was achieved using methacrylic acid modified tin(IV) isopropoxide and antimony(III) isopropoxide as precursors. Spin-on deposited films were lithographically patterned using a UV light source (I line) with a contact mask. After developing, the structures were thermally converted to crystalline, conductive pure and Sb-doped tin oxides. The effect of the UV irradiation on the chemical composition, surface morphology, and crystal size of the fabricated films was investigated using XPS, AFM, and XRD, respectively. We found that the UV irradiation lowered the crystallization temperature, increased the crystal size in the pure or slightly doped samples, and resulted in a more homogeneous Sb dopant distribution. The increase in crystal size was found to correlate with a large increase in conductivity (up to 1500%).

Introduction

Metal alkoxides are commonly modified with suitable organic ligands to reduce their reactivity against water during sol−gel processing. By an appropriate choice of the organic ligand, such as β-diketones, epoxies, or acrylics, it is also possible to fabricate directly photopatternable sol−gel-derived materials.[1,2] We have fabricated tin dioxide thin films with and without antimony doping using methacrylic acid modified tin alkoxides and antimony(III) isopropoxide as precursors.[3] These spin-coated organo-tin thin films have negative tone lithographic behavior and can be photopatterned via UV-induced (I-line) radical polymerization of the methacrylic acid ligands. After developing in 2-propanol, the organo-tin polymer structures formed can be thermally converted to conductive, crystalline pure and Sb-doped tin dioxide thin films. Interestingly, the photopatterning was found to increase the electrical conductivity of the films. The largest change in conductivity was obtained for pure SnO_2 samples (0.02 → 0.3 S/cm, 1500%), whereas the highest conductivity was achieved with UV-irradiated, 5 mol % antimony-doped samples (5.4 → 13.8 S/cm, 230%). The lowest increase was achieved with the highest doping level investigated (10 mol % Sb, 2.0 → 3.3 S/cm, which corresponds to a 60% increment). The relatively low conductivity values, compared to other values reported for sol−gel-derived antimony-doped tin dioxides,[4,5] can be attributed to the morphology of single-layer coatings.[6−8]

Directly photopatternable tin dioxide thin films are of great interest, because many applications require fine patterned transparent thin film conductors. Among such applications, for example, are transparent electrodes in display devices[8] and solar cells.[9] Tin dioxide thin films have also been of interest in gas-sensing applications.[10] Because of their high chemical durability,[2,11] fine patterning of tin dioxide thin films by wet etching is rather complicated. Recently, a new approach employing a combination of photolithographic processing of pat-

* To whom correspondence should be addressed. Tel.: +358 8 5512154. Fax: +358 8 551 2320. E-mail: Terho.Kololuoma@vtt.fi.
† VTT Electronics.
‡ Helsinki University of Technology.
§ University of Oulu.
|| VTT Information Technology.
⊥ GuideOptics Oy.

(1) Rantala, J. T.; Äyräs, P.; Levy, R.; Honkanen, S.; Descour, M. R.; Peyghambarian, N. *Opt. Lett.* **1998**, *23*, 1939.
(2) Tadanaga, K.; Owan, T.; Morinaga, J.; Urbanek, S.; Minami, T. *J. Sol-Gel Sci. Technol.* **2000**, *19*, 791.
(3) Kololuoma, T.; Kärkkäinen, A. H. O.; Rantala, J. T. *Thin Solid Films* **2002**, *408*, 128.
(4) Chatelon, J. P.; Terrier, C.; Roger, J. A. *J. Sol-Gel Sci. Technol.* **1997**, *10*, 55.
(5) Kololuoma, T.; Rantala, J. T. *Electron. Lett.* **2000**, *26*, 172.
(6) Takahashi, Y.; Wada, Y. *J. Electrochem. Soc.* **1990**, *137*, 267.
(7) Aegerter, M. A.; Reich, A.; Ganz, D.; Gasparro, G.; Pütz, J.; Krajewski, T. *J. Non-Crys. Solids* **1997**, *218*, 123.
(8) Park, S.-S.; Mackenzie, J. D. *Thin Solid Films* **1995**, *258*, 268, and references therein.
(9) Lambert, C. M. *Sol. Energy Mater.* **1981**, *6*, 1.
(10) Kohl, D. *Sens. Actuators* **1989**, *18*, 71.
(11) Tamai, T.; Ichinose, N.; Kawanishi, S.; Nishii, M.; Sasuga, T.; Hashida, I.; Mizuno, K. *Chem. Mater.* **1997**, *9*, 2674.

10.1021/cm021228j CCC: $22.00
Published on Web 09/14/2002

terned organo-tin films, followed by thermal annealing has been reported.[2,11,12] In these studies, undoped fine patterned tin dioxide thin films were prepared using relatively high UV doses[2,12] or even pulsed UV lasers.[11] Moreover, these undoped tin dioxide thin films did not gain similar UV-induced increases in conductivity, as can be seen in the samples fabricated according to our method.[3]

In this paper, we investigate the effect of UV irradiation on pure and antimony-doped tin dioxide materials derived from methacrylic acid modified tin alkoxides and antimony(III) isopropoxide. Crystallization of the antimony-doped tin dioxide materials during thermal annealing was followed by differential scanning calorimetry (DSC). Elemental analysis of the fabricated films was performed using X-ray photoelectron spectroscopy (XPS) measurements. The surface morphology of the thin films was determined using atomic force microscopy (AFM). The crystal structure and crystal size were determined by X-ray powder diffraction (XRD).

Experimental Section

To prevent the hydrolysis of alkoxide precursors by atmospheric humidity, both the modification of tin alkoxides and the preparation of the coating solutions were performed in nitrogen atmosphere. The sample preparation and all thermal treatments were carried out under class 1000 clean room conditions (T = 25 °C and RH = 45%) in ambient atmosphere.

Synthesis. Tin(IV) isopropoxide and antimony(III) isopropoxide (Chemat) were dissolved separately in 2-isopropoxyethanol (Fluka). The concentrations of the tin and antimony alkoxide solutions were 0.5 M. To obtain antimony doping levels of 0−10 mol %, appropriate amounts of the antimony alkoxide solution were added and mixed well with the tin alkoxide solution. After mixing, methacrylic acid (Aldrich) was added dropwise to the metal alkoxide solutions. The amount of added methacrylic acid was twice the amount of the tin and antimony alkoxides in terms of number of moles. Mixtures were left to react overnight. According to IR and electrospray ionization−time-of-flight (ESI−TOF) mass spectrometric analyses, both unsubstitued and mono- and dimethacrylic acid substituted tin alkoxides were formed. Before spin casting, a UV radical initiator was added to the solution (2 wt % of phenyl bis(2,4,6-trimethylbenzoyl)phosphine oxide, Irgacure 819, Ciba, vs the mass of methacrylic acid used).

Preparation of Oxide Films and Powders. Pure and antimony-doped tin dioxide thin films were fabricated by spin coating and patterned by direct UV photopatterning. Thin films were formed in a two-stage spinning process on 25 mm × 25 mm borosilicate glass substrates: (1) 5 s at 500 rpm and (2) 30 s at 1250 rpm. Immediately after being spin-coated, the films were patterned using a contact binary mask and UV irradiation (I line, 10 mW/cm^2 at 365 nm), using a UV dose of 300 mJ/cm^2. The UV-irradiated region becomes less soluble in organic solvents, which produces negative-tone lithographic behavior. After the UV exposure, the films were developed in dry 2-propanol for 30 s.

All of the spin-cast organo-tin films were first dried at 140 °C for 30 min and then annealed in ambient atmosphere to obtain crystalline tin dioxide. The highest temperature during the heat treatment of the samples was 560 °C, which was maintained for 20 min.

For DSC and XRD experiments, spin-cast specimens could not be used (the singly coated films were too thin, and the multiple coating process is known to increase the grain size[8,13]). Instead, powder samples were prepared from the coating solutions. For the UV treatment, the samples were placed on clock glasses and UV-irradiated until the solution solidified. Then, both UV-irradiated and unexposed materials were dried at 140 °C for 2 h and analyzed by DSC. For the XRD measurements, samples were sintered in porcelain crucibles under conditions similar to those used in the thin film processing.

Characterization. The behavior of unexposed and UV-irradiated powder samples under annealing was investigated using DSC. DSC analyses were carried out on a Mettler Toledo STAR instrument that consists of a DSC821 module equipped with a gas-flow-controlling system connected to the module, a pressurized gas container, and a PC using STAR software. The samples were annealed in flowing air (60 mL/min) from 25 to 600 °C at a rate of 10 °C/min. To obtain comparable DSC curves, the initial mass of the samples was kept constant at 6.3 mg.

The chemical compositions of the thin films were investigated using XPS. All experiments were recorded with a Kratos AXIS 165 electron spectrometer, using monochromatized Al Kα irradiation at 100 W. Four-kilovolt Ar^+ ions and a differentially pumped, rastering MinibeamIII ion gun were used for depth profiling. High-resolution measurements (0.1-eV step, 20-eV pass energy) were performed for surfaces only, as ion bombardment is known to change the chemical composition of oxide matrixes.[14]

The surface topology of the samples was measured using the AFM in tapping mode (Digital Instrument Dimension 3100 AFM). Areas of size 1 μm^2 were analyzed using a 0.614-Hz scan rate and a sampling density of 256 samples/line. The height data offset distortion between scan lines in the collected data was corrected mathematically by subtracting the average height value from every point in the scan line.

The crystal structure and crystal size of the fabricated powder samples were determined using XRD. XRD data were collected at room temperature (25 °C) on a Siemens D5000 powder diffractometer, equipped with a Ni filter to clear the diffractograms from Cu Kβ lines. The Cu Kα line of an X-ray source powered at 30 kV and 40 mA was used for the experiments. Samples were prepared on glass holders from ethanol suspensions. The intensity was measured by step scanning in the 2θ range between 20° and 65°, with a step of 0.02° and a measuring time of 1.3 s per point. Diffraction patterns were identified using ICDD 1999 data sets. Diffraction patterns were analyzed using the Topas P diffracplus program.[15]

Results and Discussion

DSC Measurements on Powders. DSC yields information on the behavior of a material during heat treatment. According to the DSC measurements shown in Figure 1, both the UV irradiation and the antimony doping strongly affected the annealing behavior of the material. Figure 1a and 1b presents the DSC curves for the pure and 5 mol % antimony-doped organo-tin materials, respectively, with and without UV irradiation. The third curve in Figure 1b was obtained from an unexposed sample annealed in nitrogen (N_2 flow rate 60 mL/min).

In the DCS curves, the exothermic reaction at 200 °C (seen only with unexposed, air-annealed samples) was attributed to the oxidation and liberation of methacrylic acid ligands. In the case of UV-exposed samples, the absence of this feature indicates that the methacrylic ligands were cross-linked via UV-induced radical polymerization and hence unable to leave the organo-tin polymer structure. The broad exothermic reactions at

(12) Koichi, K.; Kiichiro, S.; Katsuhiko, T.; Shinichi, H. *J. Am. Ceram. Soc.* **1999**, *82*, 2263.
(13) Schuler, T.; Aegerter, M. A. *Thin Solid Films* **1999**, *351*, 125.
(14) McIntyre, N. S.; Chan, T. C. In *Practical Surface Analysis*; Briggs, D., Seah, M. P., Eds. ; Wiley: New York, 1990; *p* 498.
(15) *Topas P*, version 1.0; Bruker AXS: Karlsruhe, Germany, 1999.

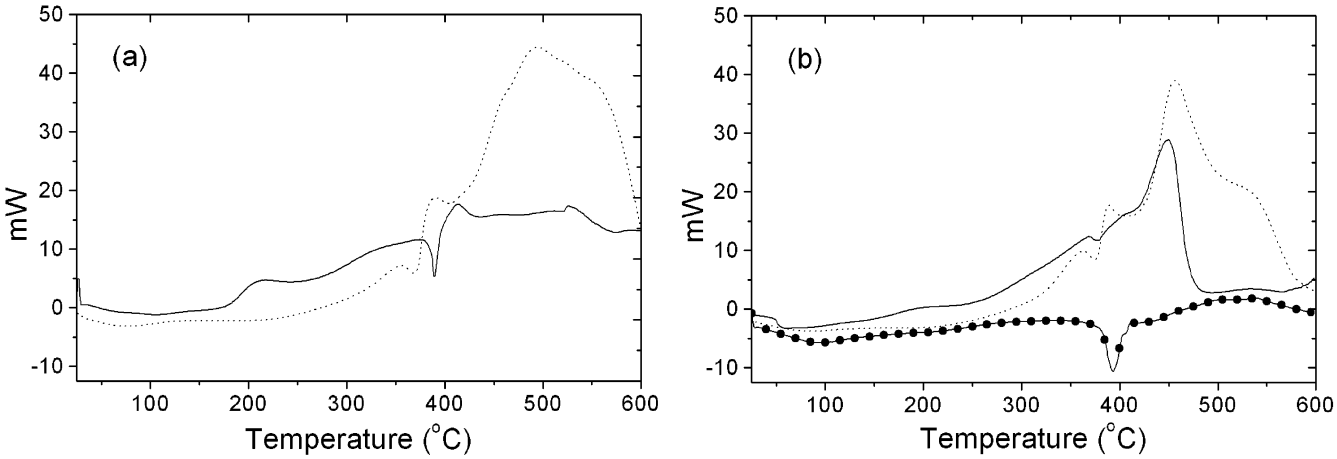

Figure 1. DSC curves of (a) an undoped organo-tin polymer annealed in air and (b) an antimony-doped (5 mol %) organo-tin polymer annealed in air (25−600 °C). (−) Unexposed sample, (···) UV-irradiated sample, and (●) unexposed sample annealed under nitrogen atmosphere (25−600 °C).

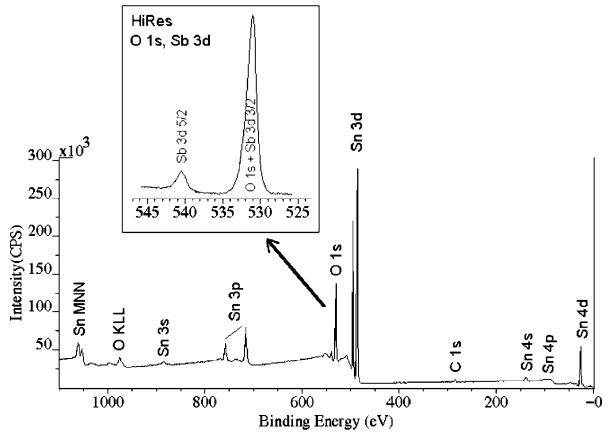

Figure 2. XPS surface spectrum of an unexposed tin dioxide thin film with 5% Sb.

250−600 °C are attributed to the oxidation and liberation of organic species (this feature was very small when the material was annealed in nitrogen). The only endothermic reaction, observed just below 400 °C in all samples, can be attributed to the decomposition of alkoxo ligands. The subsequent exothermic peak is due to crystallization of the metal oxide.

Both antimony doping and UV exposure were found to decrease the crystallization temperature. Furthermore, both Sb doping and UV treatment shifted the exothermic oxidation and liberation of organic species to temperatures higher than that required for metal oxide crystallization, although this exothermic peak is less intense for the Sb-doped samples. These DCS results indicate clearly that both the Sb doping and the UV treatment induced structural changes in the organic matrix that facilitated the crystallization.

XPS Analyses for Annealed Thin Films. Only C, O, Sb, and Sn were detected in the XPS spectra recorded from annealed film surfaces (hydrogen does not show up in XPS). As an example, in Figure 2, the wide spectrum and the O 1s high-resolution region of the unexposed sample with 5% Sb are shown. The compositions were calculated from O 1s, C 1s, Sn 3d, and Sb $3d^{3/2}$ high-resolution measurements of unsputtered specimens. Because the O 1s and Sb $3d^{5/2}$ lines superimpose, the oxygen contents were corrected using the Sb $3d^{3/2}$ line.

Table 1. Chemical Composition of Antimony-Doped Tin Dioxide Surfaces

sample	C (%)	O (%)	Sn (%)	Sb (%)	Sb/(Sn + Sb) (%)	O/(Sn + Sb) (%)
SnO_2	7	62	31.1	−	−	2
SnO_2 (UV)	6.5	61	32.2	−	−	1.9
SnO_2/Sb (1%)	8	62.5	29.4	0.35	1.2	2.1
SnO_2/Sb (1%) (UV)	10	60	29.3	0.3	1.0	2.0
SnO_2/Sb (5%)	7.5	65	26	1.55	5.6	2.4
SnO_2/Sb (5%) (UV)	5	65.5	28	1.4	4.8	2.2
SnO_2/Sb (10%)	5.5	68	23.7	2.6	9.9	2.6
SnO_2/Sb (10%) (UV)	5.5	68	24	2.4	9.1	2.6

The carbon content and the C 1s line shape were typical of surface contamination detected in air-exposed oxide surfaces. Furthermore, the C 1s line disappeared completely during the first sputter cycles. Sputter profiles for oxygen, tin, and antimony indicated homogeneous elemental distributions throughout the film, aside from the outermost surface, where the relative oxygen content was somewhat higher.

At the surface, the observed antimony contents correlated well with the nominal doping levels, as shown in Table 1. The oxygen-to-metal atomic ratio O/(Sn + Sb) was found to increase with increasing Sb doping level from 2 to 2.6. This increase is 10 times larger than the calculated value for a mixture of the respective metal oxides. However, in the doped SnO_2 lattice, each Sb ion present on the surface induces a charged surface site. These sites produce a significant increase in the surface energy of the material. Thus, the increase in O content is attributed to changes in the number of OH groups adsorbed on the surface.

Another interesting observation was that, throughout the series, both the Sb/(Sb + Sn) and the O/(Sb + Sn) ratios in the UV irradiated films were slightly lower than those in the unexposed films. These data suggest that the UV irradiation facilitated a more even distribution of Sb in the tin dioxide lattice, whereas the unexposed samples had a slight surface enrichment. This phenomenon can be explained in term of the prevention of Sb diffusion during the heat treatment of the polymerized samples.

According to the high-resolution surface measurements, Sn was present in only one chemical state. A sharp Sn $3d^{5/2}$ line at 486.8 eV is characteristic of tin dioxide.[16] The main component of the oxygen O 1s line

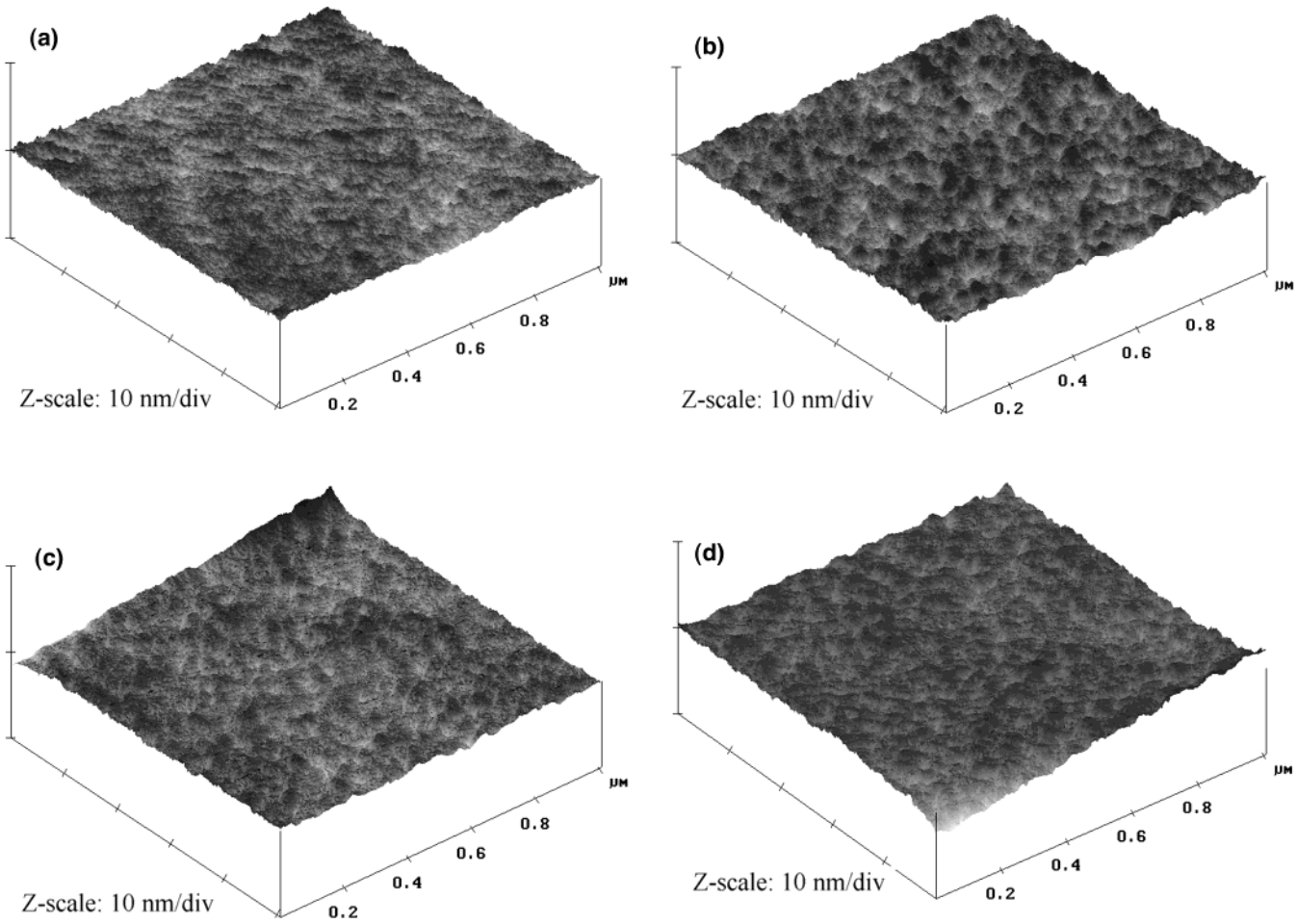

Figure 3. AFM images of the surfaces of undoped (top) and 5 mol % antimony-doped tin dioxide thin films (bottom). The *z*-axis scale is 10 nm/division in all images. (a, c) unexposed samples, (b, d) UV-irradiated samples.

at 530.5−530.9 eV is also in good agreement with tin oxides.[16] The single line of Sb $3d^{3/2}$ at 540.2 eV indicates that all antimony detected was in a pentavalent state (Sb^{5+}), which differs from the result reported by other authors.[17] In their work, antimony was reported to be in a trivalent state for low doping levels; however, they used different precursors (tin and antimony ethoxides derived from chlorides).[17]

Thin Film Surface Morphology. In Figure 3a−d, AFM images of the annealed surfaces of the undoped and 5 mol % antimony-doped tin dioxide thin films are presented.

From Figure 3a and b, it can be concluded that the UV irradiation clearly affects the surface morphology of the undoped tin dioxide surfaces. There is a small difference in the R_{rms} values of the unexposed (0.214 nm) and the UV-irradiated (0.263 nm) sample. A similar increase in R_{pv} (peak-to-valley) values is also observed, as the *z* range changes from 1.834 to 2.353 nm as a result of UV exposure. Presumably, UV irradiation assists the crystallization and the crystal growth of the undoped tin dioxide thin films and materials.

In the case of 5 mol % Sb-doped samples, AFM shows negligible grain size differences between the unexposed and UV-irradiated samples. The grain size in these samples is much like that of the exposed undoped tin dioxide film.

Thus, according to the AFM data, both antimony doping and UV exposure seem to have facilitated crystal growth. This was also indicated by the DSC data. However, only the film surfaces can be probed with AFM. To confirm the effects of UV irradiation and Sb doping on tin dioxide, XRD measurements were performed on powder specimens.

Crystal Size. According to the XRD results for the prepared powders, all samples were polycrystalline and had diffraction patterns corresponding to a SnO_2 (cassiterite) structure (Figure 4a and b). The crystal size in the samples without UV exposure was found to increase with increasing Sb doping from 10 nm (in pure tin dioxide) to 15 nm (1 mol % Sb) and 25 nm (5 mol % Sb). This result is interesting because the effect of antimony doping on SnO_2 prepared from sols without methacrylic acid ligands has been reported as the opposite.[17] On the other hand, the crystal sizes in all of the UV-irradiated samples were found to be similar, approximately 25 nm. Thus, polymerization via UV treatment was also found to facilitate crystal growth.

Thus, according to both the XRD and AFM investigations, both Sb doping and UV exposure did increase the SnO_2 grain size. According to the DCS data, both of these factors also lowered the crystallization tempera-

(16) Chastain, J.; King, R. C., Jr. *Handbook of X-ray Photoelectron Spectroscopy*; Perkin-Elmer Corporation: Eden Prairie, MN, 1995.
(17) Terrier, C.; Chatelon, J. P.; Roger, J. A.; Berjoan, R.; Dubois, C. *J. Sol-Gel Sci. Technol.* **1997**, *10*, 75.

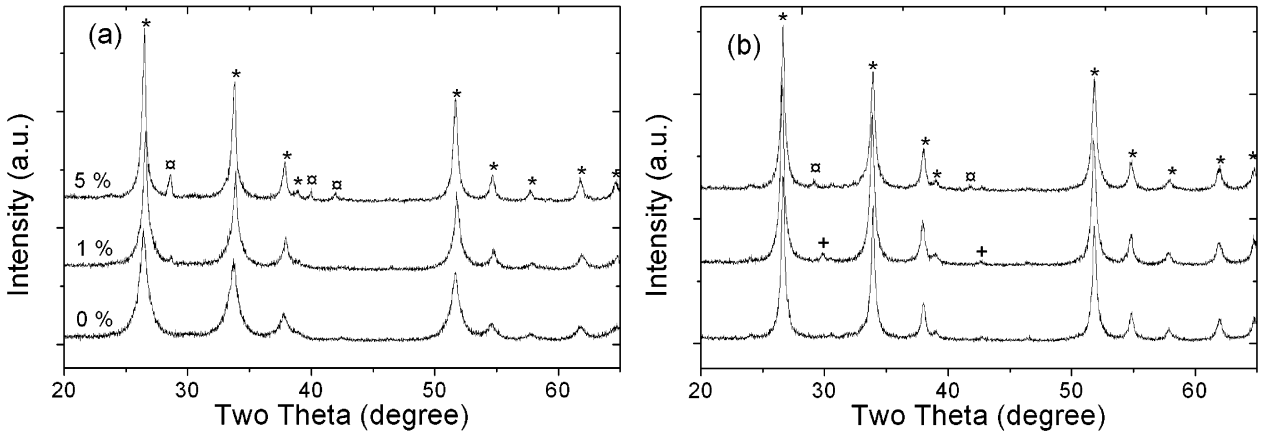

Figure 4. XRD spectra of (a) unexposed and (b) UV-irradiated pure and Sb-doped (1 and 5 mol %) tin dioxides. Patterns marked by ★, □, and + correspond to cassiterite (ICDD number 71-0652), elemental antimony (05-0562), and tin monoxide (72-1012 and 24-1342), respectively.

ture. The reaction mechanism for this phenomenon is unknown, but these experiments suggest that both polymerization via UV and the addition of antimony atoms to the system would facilitate the ordering of the methacrylic ligands into orientations more favorable for crystallization during the heat treatment. Changes in the crystal size would largely explain the observed changes in film conductivity; an increase in grain size is generally known to enhance the conductivity in semiconductor materials.

Another interesting result is revealed in the XRD data. In the case of unexposed samples, a clear diffraction pattern corresponding to elemental antimony crystallites shows up in the spectrum. The intensity of these peaks increases with increasing antimony doping level. Metallic Sb was not detected in thin film surfaces by XPS. However, during the annealing, gas-phase oxygen is quite accessible for thin film surfaces, so that all residual carbon could be oxidized, thus preventing redox reactions between metal oxides and carbon. Inside bulky powder particles, the lack of oxygen might lead to these reactions, which could result in at least partial reduction of antimony. Moreover, in the case of UV-irradiated samples, the signal from crystalline antimony is lower. This seems to indicate a more uniform antimony distribution in the grains of UV-irradiated samples, which was also indicated by the XPS surface analysis.

Conclusions

From a DSC analysis, the UV-induced polymerization of the methacrylic acid ligands was found to decrease the crystallization temperature of the pure and antimony-doped tin dioxide thin films derived from methacrylic acid modified precursors. According to AFM studies and XRD measurements, polymerization also increases the crystal size of the powder and thin film samples with low antimony doping levels. Furthermore, XPS measurements reveal that UV-induced polymerization also results in a more homogeneous antimony distribution in antimony-doped samples. According to the results obtained, the UV-irradiation-induced increase in thin film conductivity with low antimony doping levels mainly results from the increased crystal size of the fabricated materials. The relatively small increase of the electrical conductivities of the UV-irradiated samples with higher antimony doping levels is likely related to differences in the antimony distribution between the unexposed and UV-irradiated samples.

Acknowledgment. We thank Mr. O. Muhonen, Mr O. Taikina-aho, and Profs. O. Hormi and R. Laitinen for their help. Graduate School of Electronics Manufacturing is also greatly acknowledged for its financial support of T. Kololuoma.

CM021228J